

The effect of temperature and load as a stressor for proton exchange membrane fuel cells durability at intermediate temperatures

Downloaded from: https://research.chalmers.se, 2025-10-16 17:31 UTC

Citation for the original published paper (version of record):

Eriksson, B., Butori, M., Batool, M. et al (2025). The effect of temperature and load as a stressor for proton exchange membrane fuel cells

durability at intermediate temperatures. Journal of Power Sources, 658.

http://dx.doi.org/10.1016/j.jpowsour.2025.238258

N.B. When citing this work, cite the original published paper.

research.chalmers.se offers the possibility of retrieving research publications produced at Chalmers University of Technology. It covers all kind of research output: articles, dissertations, conference papers, reports etc. since 2004. research.chalmers.se is administrated and maintained by Chalmers Library

ELSEVIER

Contents lists available at ScienceDirect

Journal of Power Sources

journal homepage: www.elsevier.com/locate/jpowsour





The effect of temperature and load as a stressor for proton exchange membrane fuel cells durability at intermediate temperatures

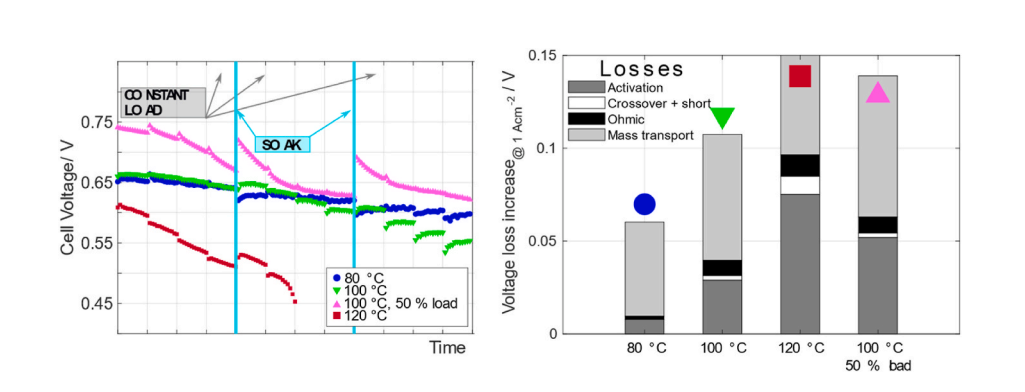
B. Eriksson ^{a,*} , M. Butori ^a , M. Batool ^b, L. Strandberg ^c , O. Sanumi ^b, S. Pedram ^b, B. Wickman ^c , J. Jankovic ^b , C. Lagergren ^a, R. Wreland Lindström ^a, G. Lindbergh ^a

HIGHLIGHTS

Ageing of PEMFCs at intermediate temperature (80–120 °C) and high load.

- Accelerated ageing at elevated temperatures.
- Main cause of performance loss is the polymer in membrane and ionomer.

GRAPHICAL ABSTRACT



ABSTRACT

To improve the Proton Exchange Membrane Fuel Cells (PEMFCs) suitability for heavy-duty vehicles a higher operating temperature is required. However, a higher operating temperature is often associated with higher degradation rates. In this work we investigate the effects of temperature and load on the degradation of commercial state-of-the-art membrane electrode assemblies (MEAs) operating at intermediate temperatures (IT) between 80 and 120 °C during galvanostatic holds. Thorough electrochemical analysis was made together with transmission electron microscopy and modelling. As expected, a more rapid decrease in performance is observed at an increased operating temperature. The main loss in performance is linked to changes in the membrane and ionomer in the membrane electrode assembly. In particular, the membranes fail due to pinhole formation, resulting in higher hydrogen crossover. It is also seen that the ionomer in the cathode degrades faster at elevated temperatures, and that a lower applied load reduces the rate. Further analysis shows small and similar changes in the electrode thickness and particle sizes for all temperatures. Although an elevated temperature reduces the lifetime of a fuel cell, operation at elevated temperatures for shorter durations can be feasible, but the polymer electrolytes must be designed for higher temperatures.

1. Introduction

The proton exchange membrane fuel cell (PEMFC) is an attractive technology due to its high energy density and could therefore be

employed in the electrification of heavy-duty vehicles (HDVs) and other demanding applications e.g., marine and air transportation. As waste heat rejection is simpler at higher operating temperatures, an elevated operating temperature, up to 120 $^{\circ}\text{C}$ is desirable, at least at increased

https://doi.org/10.1016/j.jpowsour.2025.238258

^a Dept. of Chemical Engineering / Applied Electrochemistry, KTH Royal Institute of Technology, SE-100 44, Stockholm, Sweden

^b Materials Science and Engineering Department, University of Connecticut, Storrs, CT, 06269-3136, USA

^c Department of Physics and Competence Centre for Catalysis, Chalmers University of Technology, SE-412 96, Göteborg, Sweden

^{*} Corresponding author. *E-mail address*: bjorerik@kth.se (B. Eriksson).

power demands [1–3]. However, given the much longer lifetime expected for HDVs (30 000 h) compared to light-duty vehicles (LDVs, 8000 h), much more attention must be paid in minimizing the degradation of the cell [1].

Among proton exchange membranes (PEMs), the most used membrane is Nafion, or similar perfluorosulfonic acid (PFSA) membranes [4–6]. The degradation mechanisms of such membranes have been studied extensively. In general, there are three main types of membrane degradation: thermal degradation, mechanical stress, or chemical degradation [4,5,7,8]. All types of losses in membrane properties can lead to changes in the ionic conductivity or in the mechanical strength of the membranes. Pinholes are of particular importance, as their formation can lead to a downward spiral of increased crossover and accelerated degradation [9–11]. Stressors for chemical membrane degradation include low humidity and elevated temperatures [7]. Elevated temperatures can also lead to irreversible mechanical changes, and membrane creep, as the glass transition temperature of Nafion is around 100 °C [12, 13].

Another key-component together with PEMs in membrane electrode assemblies (MEAs) for PEMFCs is the catalyst layer. It mainly consists of the catalyst material, usually Pt nanoparticles, ionomer (an ionconductive polymer with similar properties as the membrane) and the catalyst support, most often carbon particles. Performance loss in the electrode can be caused by degradation of any of these components. The typical degradation mechanism of the catalyst is Pt dissolution, detachment with consequent coalescence, migration, or Ostwald ripening mechanism [11,14-16]. All these types of Pt degradation led to a loss of electrochemical surface area (ECSA) which directly causes a decrease in performance. Pt dissolution can also lead to Pt diffusion into the membrane [17]. While the degradation of the Pt catalysts is predicted to occur at high cathode potentials close to open circuit voltage (OCV), experiments have shown the occurrence of Pt degradation at operational fuel cell voltages (\sim 0.75 V) [16,17]. The degradation of the ionomer follows similar mechanisms as the membrane [11]. Degradation of the carbon support is caused by the reaction of carbon with water, with a standard potential of 0.207 V vs normal hydrogen electrode (NHE) [18,19]. However, due to the slow kinetics the reaction occurs mainly at potentials above 1.1 V, but in the presence of Pt catalyst effects can be seen at a potential as low as 0.55 V [19].

Few studies have measured PEMFC degradation at elevated temperatures. Kakinuma et al. [13] used OCV hold to investigate membrane ageing of Nafion and noted that at 120 °C the membrane degradation occurred 5 times faster compared to at 90 °C. They utilized voltage cycling between 0.6 and 1.0 V and observed a retention of only 16 % of the electrochemical surface area (ECSA) at 120 °C compared to 46 % at 80 °C, while also noting an increase of particle size from 3 nm to 7.6 and 5.7 nm respectively. During the voltage cycling, lowering the humidity from 80 % to 20 % increased the ECSA retention to 77 % and limited the average particle size to 4.4 nm. Another study by Mathias et al. [2] underlined that after 5000 cycles at 25 % RH between 0.7 and 0.9 V, the ECSA loss was 10 % at 80 °C and 20 % at 120 °C, suggesting that while a higher temperature caused an increase in ECSA loss it did not hinder the overall performance substantially.

Accelerated stress tests (ASTs), including those abovementioned, are often utilized to facilitate faster testing of ageing. However, it has been pointed out that ASTs on a single component might be more aggressive than the operation in actual applications, thanks to the mitigation strategies that are currently adopted in fuel cell vehicles [20]. Alternatively, load cycling protocols can be employed to reproduce typical degradation modes of a cell subjected to driving conditions, such as the New European driving cycle (NEDC), which include stressors such as higher temperatures [21]. The ID-FAST H2020 European project developed a new AST for fuel cell based on real-life driving data, where most of the drive cycle is conducted at 71 °C but the high power is done at 90 °C. They noted significant different ageing modes for three different CCMs tested, suggesting the importance of CCM design.

However, no comparison with a constant temperature was given, making it difficult to fully understand the effects of operating temperature [22,23].

Few studies have investigated the effects of higher temperatures on the degradation of fuel cells, and none have measured more than one temperature above 80 °C and under constant load. In this study, galvanostatic measurements at high power and 80, 100 or 120 °C are used to investigate the effect of temperature and load on the ageing in PEMFCs. Measurements are done while periodically performing electrochemical characterizations including cyclic voltammetry, electrochemical impedance spectroscopy and polarization measurements, to be able to systematically analyze the degradation. In addition, cross-section TEM post analysis is used to investigate changes in the catalyst layer in detail. A 0-D model is employed to better understand the different losses occurring in the fuel cell.

2. Experimental

2.1. Setup

The cell house (Fuel Cell Technologies), with a 5 cm² serpentine flow field, was mounted in a fuel cell setup containing two humidifiers (Fuel Cell Technologies), two mass flow controllers (Brooks 5850E) and two manual back-pressure regulators (Fairchild 3024BP). The temperatures of the humidifiers, pipes and cell house were controlled using PID controllers (Eurotherm 3216). For the CO-stripping measurements, an additional flow controller (Bronkhorst EL-FLOW Select) was used to supply dry 2 % CO in Ar at the cathode side. For all measurements, a commercial MEA with anode and cathode loadings of 0.1 and 0.2 $\rm mg_{Pt}$ cm $^{-2}$ and a 10- μ m-thick reinforced PFSA membrane was utilized. The gas diffusion layer (GDL) used was made of carbon paper with a thickness of 220 μ m (including the microporous layer) and a 200- μ m-thick PTFE sheet was employed as gasket on each side. The cell was compressed using 10 Nm of torque.

For each sample a reference condition (RC: 80 °C and 70 % RH, same for all sample) and a setpoint condition (SP: 80/100/120 °C and 70 % RH, depending on the sample) were utilized. A total pressure of 3.1 bar (abs.) and 3.0 bar (abs) was used at the anode and cathode, respectively. As shown in our previous work, the use of both high humidity and high total pressure permits us to achieve high performance at higher temperatures [24]. While the SP conditions were employed for the ageing protocol, the RC was employed to characterize the cell at the beginning of the test and every 48 h, allowing the comparison of the cell ageing at different temperatures, as described in Table 1. A detailed table with all the measurement steps is shown in the SI. Two different samples were tested for each temperature condition. Additionally, at SP = 100 °C, two samples were further tested applying half of the load.

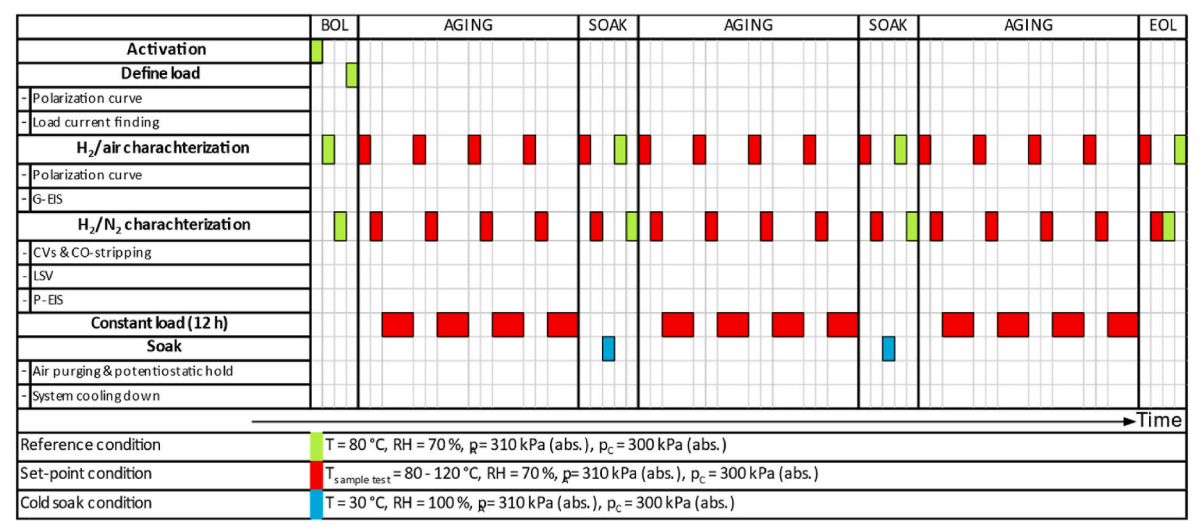
The measurements were performed using the anode as reference and counter electrode, and the cathode as working electrode. The measured cell voltage (E_{cell}) between anode and cathode is used for plotting the polarization curves.

2.2. Electrochemical measurements

All electrochemical measurements were performed using a GSTAT302N Potentiostat (Metrohm Autolab) with a BSTR10A booster (Metrohm Autolab). At each condition two individual measurements were performed. For each measurement, the following procedure was utilized. Firstly, an activation procedure was carried out at the RC. The cell was activated by galvanostatic holds from 0.1 to 0.9 A cm $^{-2}$ (with 0.1 A cm $^{-2}$ steps) for 45 min, followed by a hold at 1.0 A cm $^{-2}$ for 2 h. Then, a complete electrochemical cell characterization was carried out: under $\rm H_2/air$, a polarization curve and galvanostatic electrochemical impedance spectroscopy (G-EIS) measurements were performed, while under $\rm H_2/N_2$, CO-stripping voltammetry (after flushing dry 2 % CO in Ar at the cathode side), potentiostatic electrochemical impedance

Table 1

Outline of the experimental protocol. The sequence of each condition, marked with a color for set point (SP) reference condition (RC) and cold soak, is displayed on a time axis of totally 144 h. In the final characterization no cold soak was performed. Further details are provided in the SI.



spectroscopy (P-EIS) and linear sweep voltammetry (LSV) were measured. The former characterization is indicated in the result section as beginning of life (BOL) characterization at the RC. During the characterization a constant flow of 265 ml min $^{-1}$ H $_{\rm 2}$ and 662 ml min $^{-1}$ air were used, this corresponds to 3.5 times the stoichiometric requirement at 10 A. For the ageing an excess of 2.5 of the stoichiometric requirement was maintained.

Polarization curves were recorded by galvanostatic holds at currents from 0.4 to 100 mA cm $^{-2}$ in steps for 1 min, then from 200 to 1400 mA cm $^{-2}$ for 2 min each. The steps were then repeated in reverse. G-EIS was performed with DC currents from 10 to 1200 mA cm $^{-2}$ from 100 kHz to 0.1 Hz, with an AC amplitude of 5 % of the applied DC current. The HFR was obtained from the real part of the impedance when the imaginary part was 0 at high frequencies.

The P-EIS under $\rm H_2/N_2$ were carried out from 100 kHz to 0.1 Hz with an applied DC voltage of 0.4 V and an AC amplitude of 5 mV. The ionic resistance of the ionomer was obtained by calculating three times the distance between the HFR and the value of the real part of the impedance once the phase angle was above 45° [25].

The cyclic voltammetry (CV) was carried out by sweeping the potential from either 0.1–0.8 V (at SP) or to 1.2 V (at RC) with a sweep rate of 20 mV s $^{-1}$ for five cycles. The lower upper potential at the setpoint condition was chosen to avoid carbon corrosion and Pt degradation during the characterization. First, 50 ml min $^{-1}$ of 2 % CO in Ar was supplied for 2 min, afterwards N_2 was flushed for 8 min to remove any remaining CO. During this time the potential was held at 0.15 V to avoid any oxidation of the bound CO. Afterwards the CO-stripping was performed similarly to the baseline CV. The ECSA was then obtained from the subtraction of the additional charge due to the CO stripping and divided by the specific charge of 420 μ C cm $^{-2}$ [26]. The peak position and full width half maximum (FWHM) of the CO peak was obtained by fitting a gaussian curve.

The LSV was carried out by sweeping the potential from 0.1 V to 0.7 V with a sweep rate of 0.1 mV s $^{-1}$. The hydrogen crossover current was obtained from the linear extrapolation of the values from 0.4 to 0.6 V $^{-0}$ V.

The cell was then heated to the SP condition over 1 h. Once the SP was reached, similar cell characterizations were performed, which is indicated in the results as BOL characterization at the SP. The long heating time was used to ensure that steady state has been reached prior

to the electrochemical measurements. Then the cell was run at SP conditions by applying a constant current for 144 h corresponding to the current obtained at 0.65 V at the RC initially measured about 1.3 A cm⁻², which is considered 100 % load as is detailed in the EU harmonized protocols [21]. If the cell voltage went below 0.1 V during the galvanostatic measurement, the measurement was terminated and the "end of life" EOL characterization was initialized. For the measurements done at 50 % load, the current obtained at 0.65 V was halved prior to being applied, around 0.65 A cm⁻². After every 12 h of operation, a complete cell characterization at SP was performed. After every 48 h a shutdown procedure was performed, here called "cold soak". During this the cell was cooled to 30 °C for 8 h and the humidifiers' temperature was set to 30 °C (100 % RH). Afterwards the cell was heated to RC where cell characterization was performed and then heated to SP where an additional characterization was performed. The last characterization at SP and RC are indicated as EOL characterizations. No cold soak was done before the characterization at RC for the EOL. A detailed table with all the measurement steps is shown in the SI.

2.3. Microscopy evaluation

To visulaize and quantify changes in the cathode catalyst layers during degradation, fresh and tested MEAs were characterized by S/TEM-EDS microscopy using a Talos F200X microscope (Thermo Fisher Scientific, USA), at the University of Connecticut. To prepare the samples, small pieces of MEAs were embedded in a 1:1 mixture of 4,4'-Methylenebis (2-methylcyclohexylamine, Sigma-Aldrich, USA) hardener and trimethylolpropane triglycidyl ether resin (Sigma Aldrich, USA), microtomed to thin (~100 nm) slices using Leica UCT ultramicrotome (Germany), and placed on Cu/Pd TEM grids. Brigh field imaging was performed to collect images at 190 kx magnification and evaluate Pt particle size distribution (PSD). In-house developed deep learning-based approach was used to measure thousands of particles in a number of areas and provide Pt PSD and mean particle size [28]. STE-M-EDS elemental mapping at 5 kx and 79 kx magnification was used to map the distribution of Pt catalyst, carbon support and ionomer (following fluorine signal) in the cathode, and evaluate if any changes occurred during testing. The elemental maps were visualized using ESPIRIT 1.9 (Bruker, USA) analytical software. An in-house developed EDS maps quantification method was used to provide Pt loading, I/C ratio and porosity of the samples [29,30].

The membrane thickness was obtained through cross section with SEM/EDX (Hitachi 2–4800/X-MaxN 80 Silicon Drift Detector (SDD), Oxford Instruments).

2.4. Model for estimation of polarization losses

To estimate the losses in the polarization, a 0-D model similar to that proposed by Joui et al. [27] was utilized:

$$\begin{split} E_{cell} = & E_{rev} - k_t \left(T - T_{ref} \right) + \frac{RT}{nF} \ln \left(p_{H_2} p_{O_2}^{\frac{1}{2}} \right) - \frac{RT}{\alpha nF} \ln \left(\frac{i_{loss} + i}{i_0} \right) - i^* HFR(T, RH, i) \\ & - B_c \ln \left(\frac{i_L}{i_L - i} \right) \end{split}$$

[Eq. 1]

Where E_{rev} is the reversible potential, k_t is the shift in standard potential due to temperature and is 0.85 mV K $^{-1}$, T_{ref} is the reference temperature of 273 K, T is the cell temperature (in K), R is the gas constant, F is Faraday's constant, n is the number of electrons per mole of reactant, p_{H_2} and p_{O_2} are the partial pressures of hydrogen and oxygen, α is the charge transfer coefficient, i_{loss} is the hydrogen crossover and the short circuit current measured from the LSV, HFR(T, RH, i) is the high frequency intercept from the G-EIS, B_C is an empirical parameter to consider non-uniform current densities in the electrode and i_L is the limiting current density [27].

When fitting the model to the data i_0 , i_L and B_C were fitted while the remaining variables were taken from the other characterizations and α was kept at 0.5.

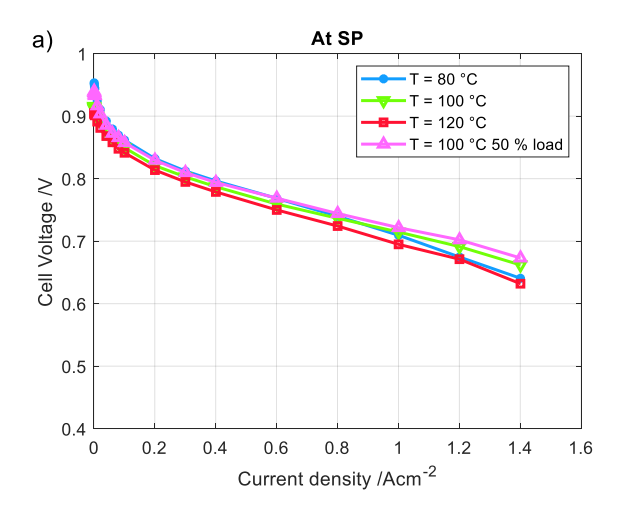
3. Results and discussion

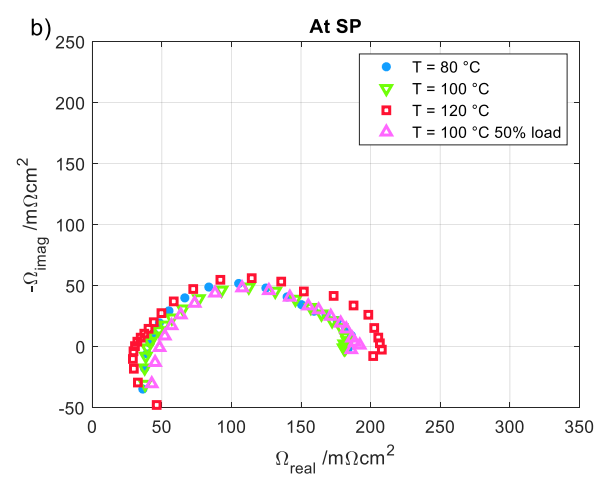
3.1. Effect of temperature at cell level at beginning of life (BOL)

The initial performance and characterization for one of the samples tested at each condition are shown in Fig. 1. All samples have similar performance at the reference condition (RC) of 80 °C (Fig. S1), and even at different temperatures (Fig. 1a), only a slight deviation at higher current densities is observed. The tested samples are from the same sheet of commercial MEA and as such good reproducibility at BOL is expected. The small loss at higher temperatures is a consequence of the oxygen partial pressure being the most important parameter to have good performance if the relative humidity is the same, as shown in our previous study [24]. In this study, due to the high back pressure of 3 bar absolute, a high oxygen partial pressure can be obtained even at 120 °C. Although the water partial pressure increases with temperature, the oxygen gas partial pressure is still sufficient for operation, reaching 56, 48 and 34 kPa (abs.) at 80, 100 and 120 °C and 70 % RH respectively.

The G-EIS measurements shown in Fig. 1b (and Fig. S1b), are similar at both RC and SP. All samples initially show comparable high frequency resistance (HFR), suggesting that the initial membrane conductivity is the same for all samples. However, the low frequency resistance (LFR) for the 120 $^{\circ}\text{C}$ sample is slightly higher compared to the other samples, which is most likely the cause of the reduced initial performance seen in the polarization curve.

Finally, the CO-stripping curves (Fig. 1c) show that all samples have similar ECSA at the beginning of the test at both RC and SP. At elevated temperatures a shift of the CO oxidation peak to lower potentials with an increasing temperature is observed, which is expected due to the lowering of the onset potential for CO oxidation at elevated temperatures [31,32]. However, as the measured ECSA was similar, the CO-stripping is assumed to be valid for the remaining analysis taken at the different temperatures. Overall, it can be confirmed that at BOL all samples are reasonably similar and have performance both at the RC and at the SP.





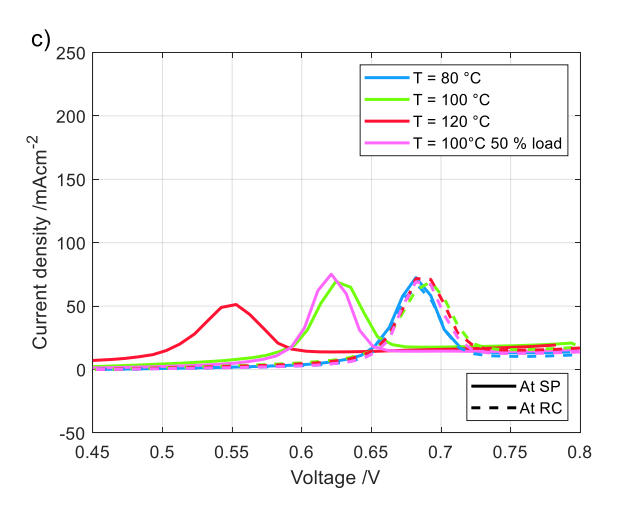


Fig. 1. a) Polarization curves, b) G-EIS at 0.6 A cm $^{-2}$, c) CO-stripping curves at the SP of 80, 100 or 120 °C. Measurements were done at 70 % RH, 3 bar absolute pressure, with 265 ml min $^{-1}$ of H₂ and 662 ml min $^{-1}$ of (a–b) air or (c) N₂.

3.2. Effect of temperature and load on performance decay

In Fig. 2a the cell voltage evolution during the constant load measurements is summarized. The graphs show that the cell voltage decreases with time for all temperatures and loads. The repetition for each condition is shown in the supplementary data. Fig. S4 shows that the variation between samples is large. However, the trend with rising

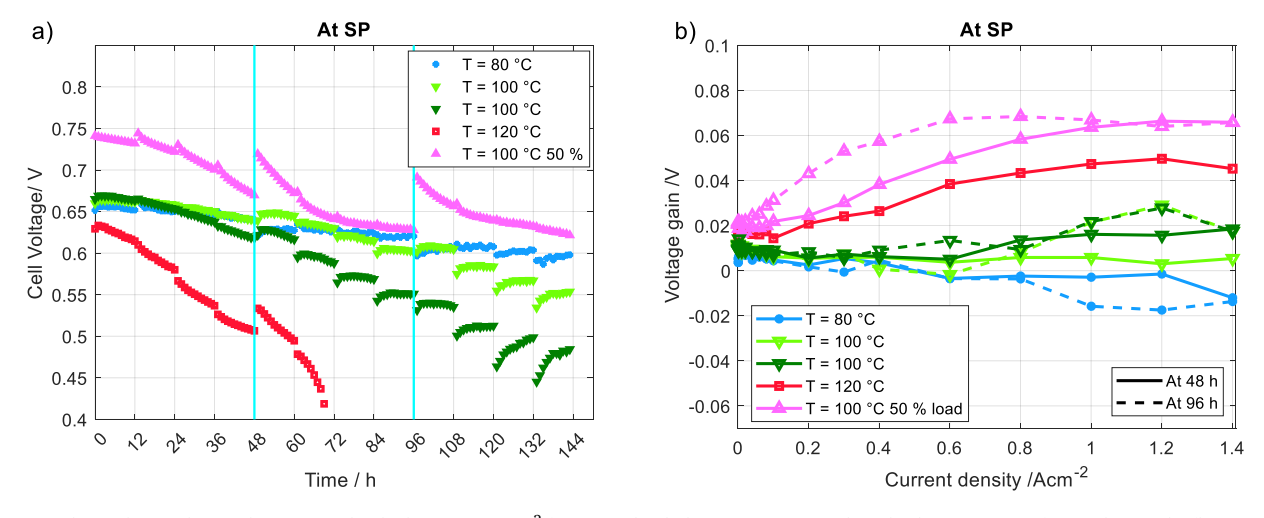


Fig. 2. a) Voltage change during the constant load, about 1.3 A cm $^{-2}$ for 100 % load, done at 70 % RH, 3 bar absolute pressure of $\rm H_2$ and air and a flow rate 2.5 times the stoichiometric requirement. Every 12 h the constant load is interrupted for characterization. Cyan vertical lines indicate the execution of a cold soak. b) Gain in the cell voltage of the polarization curves recorded after the cold soak compared to before. Measurements were done at 70 % RH, 3 bar absolute pressure and with $\rm H_2$ and air flow rates of 265 ml min $^{-1}$ and 662 ml min $^{-1}$. (For interpretation of the references to color in this figure legend, the reader is referred to the Web version of this article.)

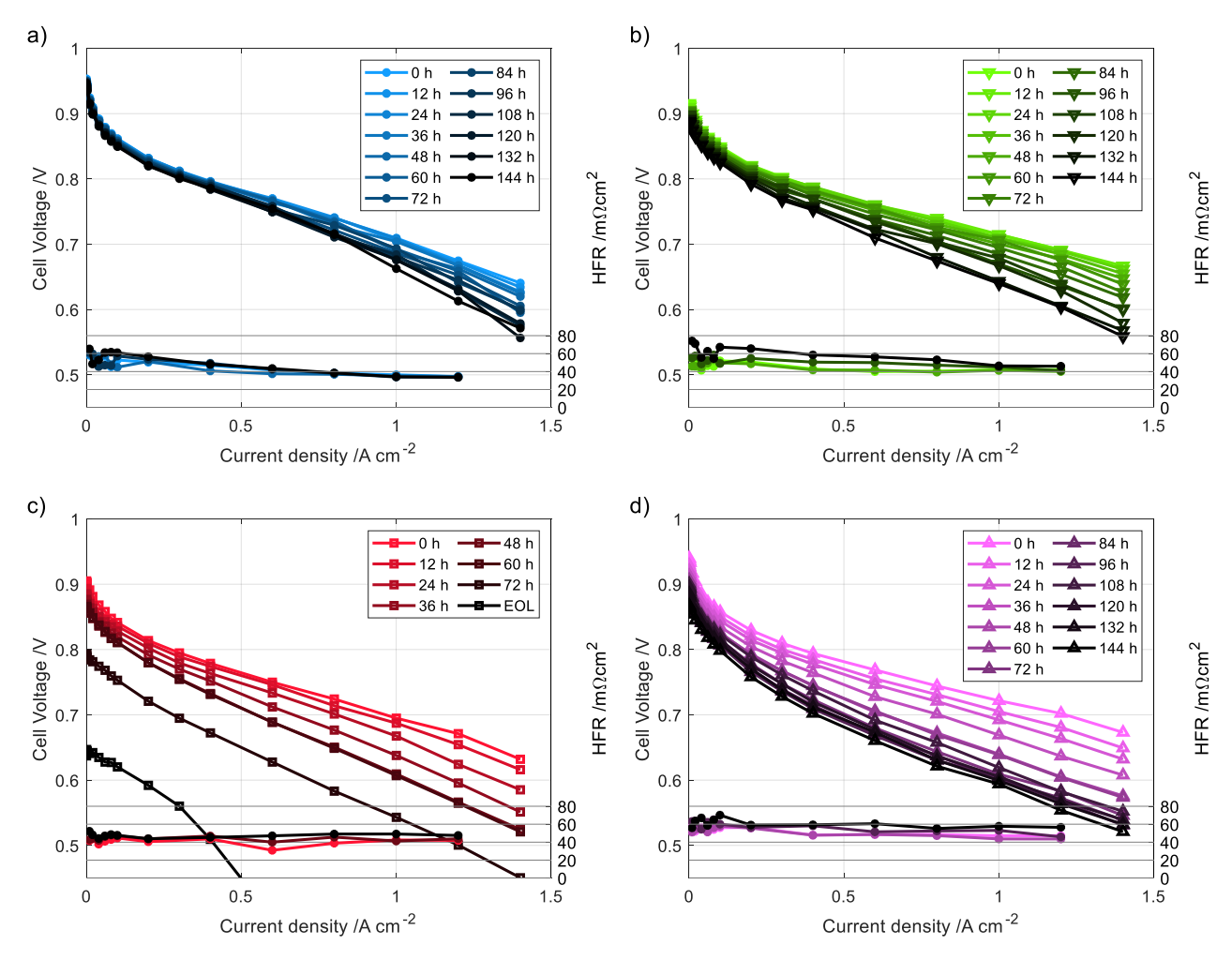


Fig. 3. Polarization curves and HFR over time at SP: a) 80, b) and d) 100, and c) 120 °C and 100 % load (a,b,c) and 50 % load (d). Measurements were done at 70 % RH, 3 bar absolute pressure, with $\rm H_2$ and air with flow rates of 265 ml min $^{-1}$ and 662 ml min $^{-1}$. For the sample at 120 °C the EOL was reached after 72 h (during the characterization).

temperature is the same. Every 12 h the characterization is performed, which causes a slight negative shift in the cell voltage, in all cases except for the 50 % load. The decrease partially recovers after a couple of hours at SP, but it is still evident that the characterization steps caused some irreversible changes. The cold soak performed every 48 h, shown in Fig. 2b, caused an improvement in cell voltage for the $100\,^{\circ}\text{C}$ and $120\,^{\circ}\text{C}$ sample, likely due to increased wetting of the polymer, while causing a decrease for the $80\,^{\circ}\text{C}$ sample. It is important to note that both the samples aged at $120\,^{\circ}\text{C}$ failed after around 72 h and could not be tested further, unlike all the other operating conditions which lasted the full 144 h test. At $100\,^{\circ}\text{C}$ a relatively large variation between the duplicates is observed after the first cold soak.

To determine if a lower load could lead to slower ageing, measurements with only 50 % applied load (\sim 0.65 A cm $^{-2}$) were performed at 100 °C as well. Due to the lower applied current density, the 50 % load sample has a higher operational voltage of \sim 0.75 V instead of \sim 0.65 V. It can be noted that the characterization each 12 h and cold soak each 48 h have a positive effect on the cell voltage for the half-load sample. This suggests that significant parts of the voltage loss at 50 % load are reversible and that the samples suffer from insufficient humidification.

The polarization curves at SP every 12 h are shown in Fig. 3. After being aged at constant current, and been subjected to characterization, a lower cell voltage at high current densities is observed for all samples. In particular, the sample run at 80 °C, Fig. 3a, shows almost negligible ageing in the low current density region, while it is affected by a more

pronounced mass transport loss at current densities above 0.6 A cm⁻².

The samples aged at 100 °C (Fig. 3b) and 120 °C (Fig. 3c) and full load present a different ageing behavior compared to 80 °C. Firstly, a loss in the OCV is observed, most likely due to increased hydrogen crossover. Additionally, a clear shift to lower potentials is observed for the entire current density range. From the polarization curve it is obvious that a pinhole has started to form between 60 and 72 h in the $120\ ^{\circ}$ C sample.

The samples aged at 100 °C using half of the load (Fig. 3d) have a higher loss of performance compared to the full load when measured at the SP (and at the RC, Fig. S5). This could be due to the fact that the cell is maintained at a higher potential of 0.74 V at 50 % load compared to 0.66 V at 100 % load, which is more detrimental for the catalyst and support [11]. In accordance with Fig. 1b higher HFR values are observed for higher temperatures. For all samples a general trend of higher currents causes a slight decrease in HFR. The change in HFR with current is less pronounced at higher operating temperatures as the self-humidification from produced water is reduced.

At the EOL the decrease in cell voltage at $1~\rm A~cm^{-2}$ is 7.2 %, 11.8 % and 21.7 % for 80, 100 and 120 °C. For the sample at 100 °C and half load the loss in potential was 15.2 %. For 120 °C EOL is measured at 72 h from the beginning compared to 144 h for the remaining samples. It should be noted that HFR, associated with membrane resistance, is independent of load. Further, the HFR tends to diminish at lower current and lower temperatures, while it is more independent on the current

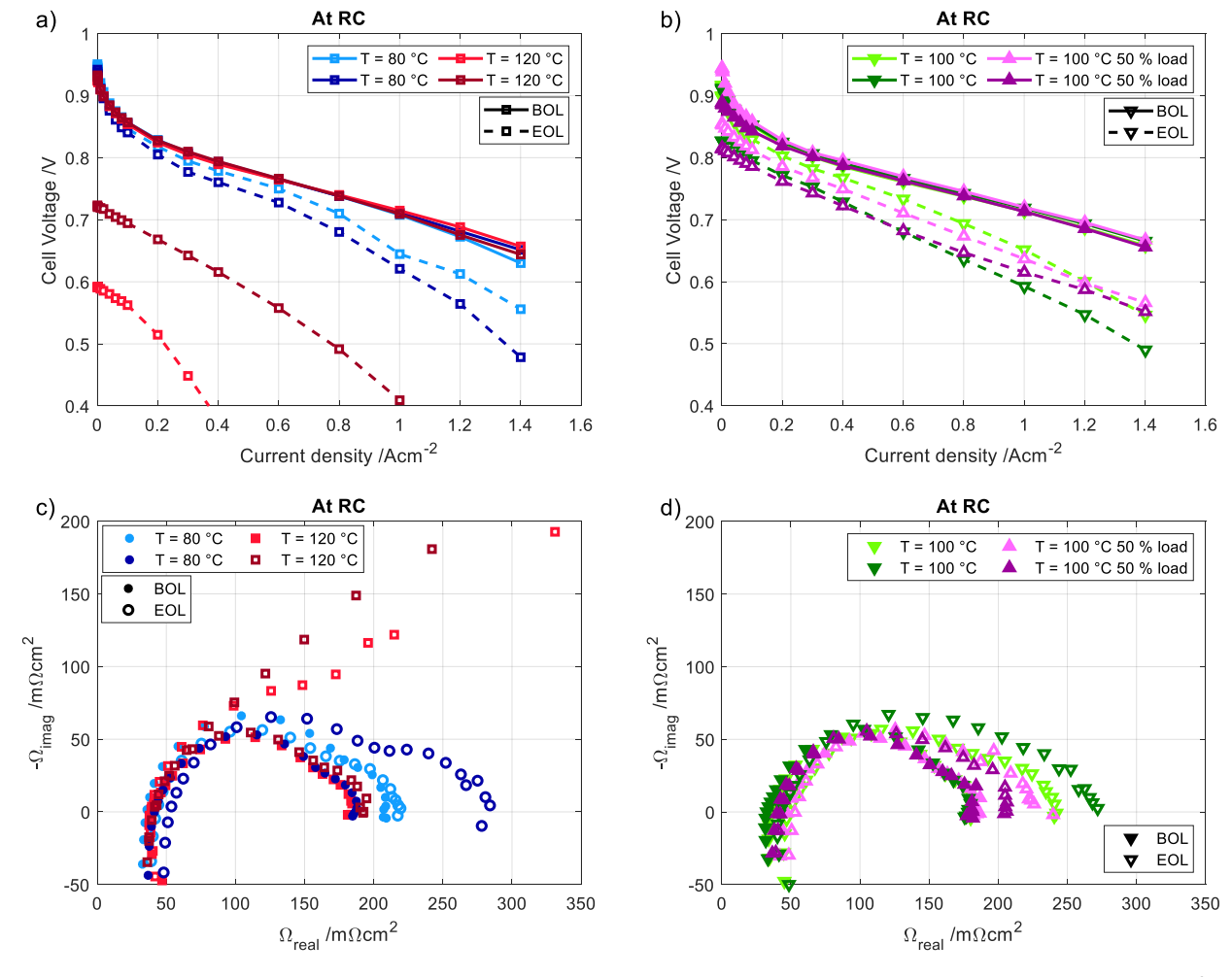


Fig. 4. Polarization curves a) 80 and 120 $^{\circ}$ C at 100 $^{\circ}$ C load and b) 100 $^{\circ}$ C for 100 and 50 $^{\circ}$ 6 load and galvanostatic impedance spectroscopy at 0.6 A cm $^{-2}$ for c) 80 and 120 $^{\circ}$ C at 100 $^{\circ}$ 6 load and d) 100 $^{\circ}$ C for 100 and 50 $^{\circ}$ 6 load. Measurements were done at reference conditions (RC) 70 $^{\circ}$ 8 RH, 3 bar ab pressure, with 265 ml min $^{-1}$ H₂ and 662 ml min $^{-1}$ 9 of air.

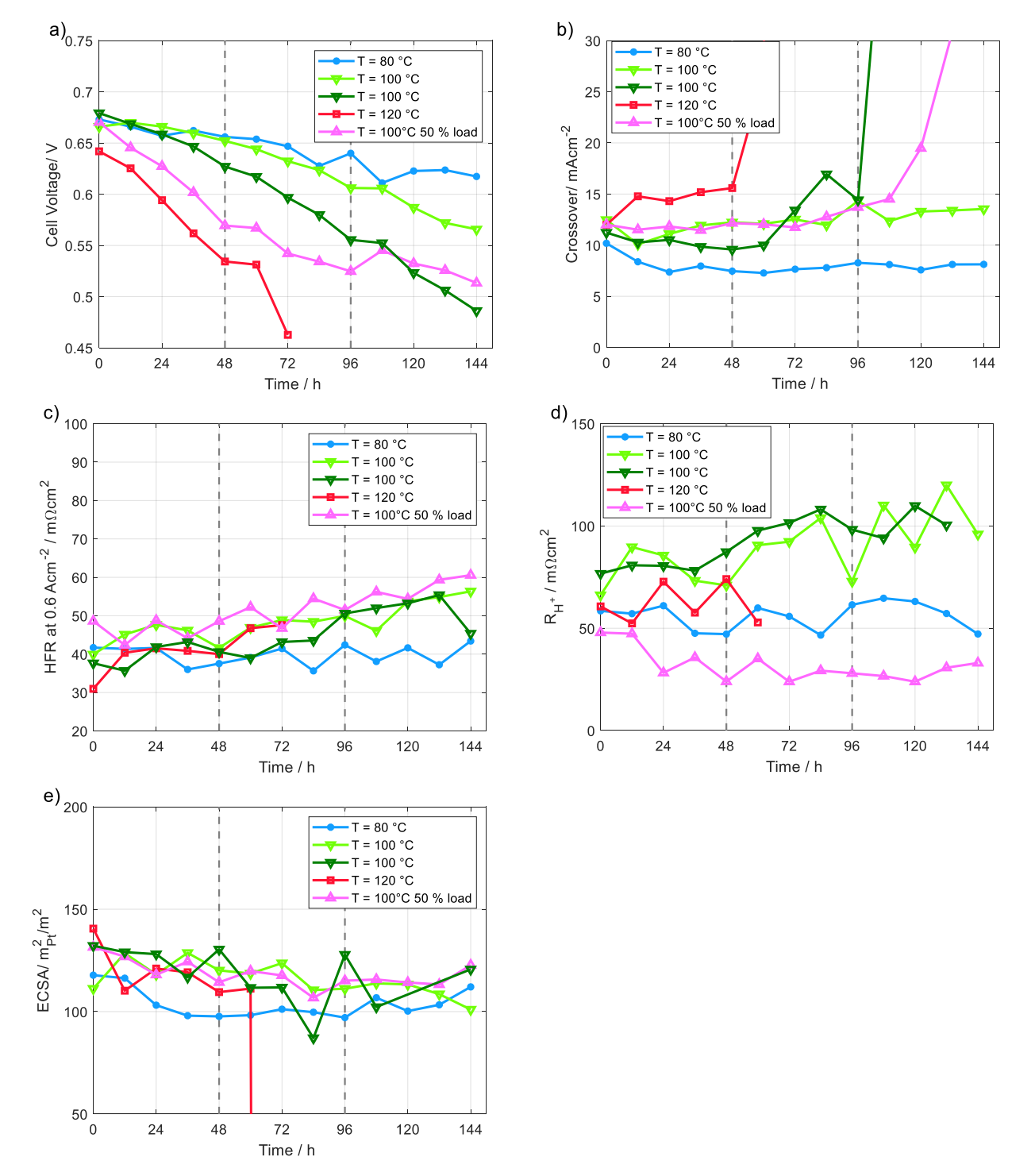


Fig. 5. Changes of a) cell voltage during load, b) hydrogen crossover, c) high frequency resistance (HFR) at 0.6 A cm⁻², d) cathode ionomer resistance, and e) electrochemical active surface area (ECSA) over time. Measurements were done at setpoint conditions (SP). Repetitions and measurements done at reference conditions can be found in the SI.

level at higher temperature.

To understand the cause of the performance losses recorded throughout the ageing tests, characterizations were performed every 12 h at the SP and at the same temperature (RC) every 48 h. A comparison between the BOL and EOL measurements at RC of 80 $^{\circ}\text{C}$ is shown in Fig. 4. Although the ageing behaviors within the repetition of the same test were similar; to provide a more quantitative analysis, the two tests performed for each operating condition are plotted in the following figures.

From the polarization curves, Fig. 4a and b, it can be seen that at the comparable RC the ageing becomes more severe at higher temperatures. Compared to the BOL and EOL curves at SP shown in Fig. 3, at RC similar observations regarding the influence of temperature and load can be made in Fig. 4a and b.

The $\rm H_2$ and air G-EIS measurements at 0.6 A cm $^{-2}$, plotted in Fig. 4c and d, show that all samples have similar HFR and semicircle height. Main difference is an increase of the low frequency intercept, which is associated with an increase in the mass transport resistance. At 120 °C, it

Table 2Data obtained from the STEM-EDS analysis on one fresh sample and one aged sample for each operating condition.

	Cathode Fres	80 °C	100 °C	100 °C–50 %	120 °C	Average for all
Total porosity, %	77	72	67	71	71	70
Pt loading, mg/cm ²	0.28	0.28	0.28	0.3	0.26	0.28
Pt particle size (±distribution), nm	$4.74(\pm0.12)$	$5.2(\pm 0.135)$	$5.25(\pm0.135)$	$5.32(\pm0.140)$	$5.12(\pm 0.137)$	$5.22(\pm 0.14)$
Ionomer loading, mg/cm ²	0.18	0.23	0.26	0.23	0.30	0.26
I/C	1.03	1.38	1.22	1.78	2.23	1.65
Layer thickness, um	8.11	7.52	7.5	6.58	7.84	7.36

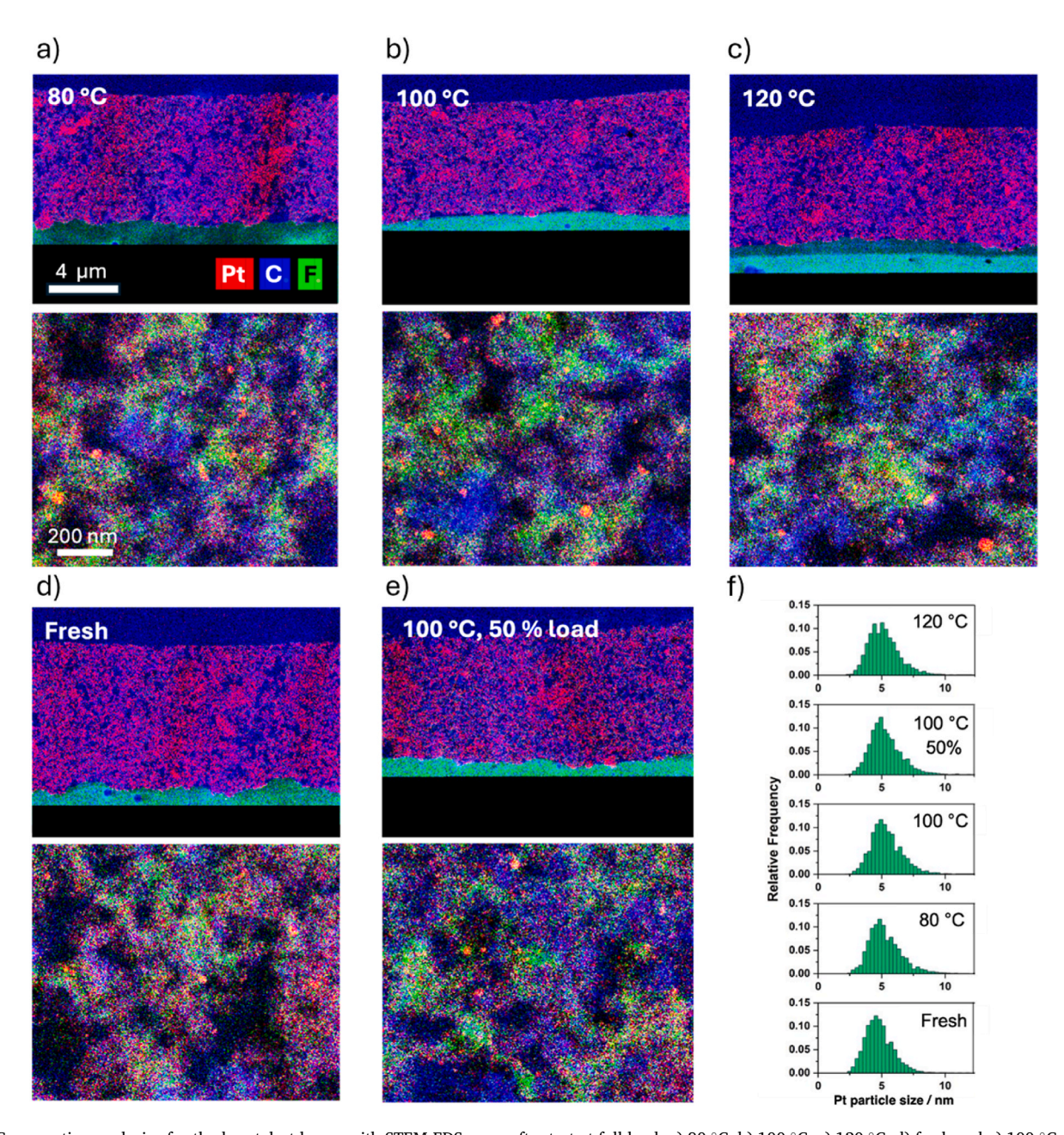
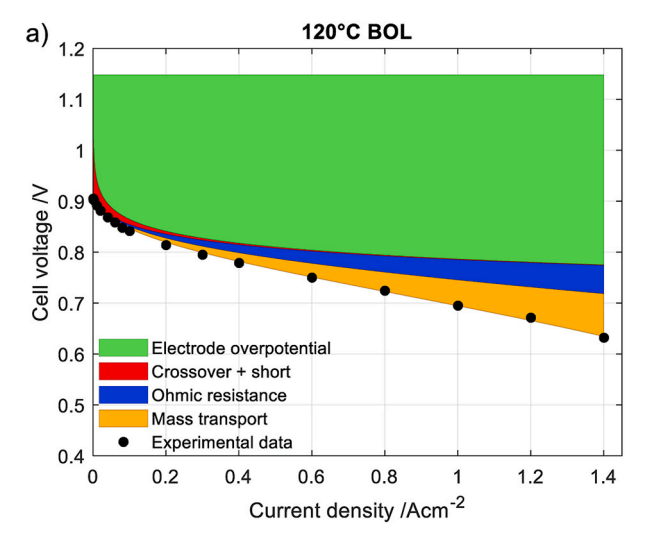


Fig. 6. Cross-section analysis of cathode catalyst layers with STEM-EDS maps after test at full load. a) 80 °C, b) 100 °C, c) 120 °C, d) fresh and e) 100 °C and 50 % load. Upper micrograph shows the entire catalyst layer thickness and beneath is a larger magnification for a detailed view of the catalyst layer structure. The corresponding images for the different conditions has the same magnifications. The colors indicate Pt (red), C (blue) and F (green). The membranes, shown in green at the bottom of the upper micrograph were not mapped fully and should not be considered here. f) Pt particle size distributions close to the membrane obtained from bright field TEM images. (For interpretation of the references to color in this figure legend, the reader is referred to the Web version of this article.)



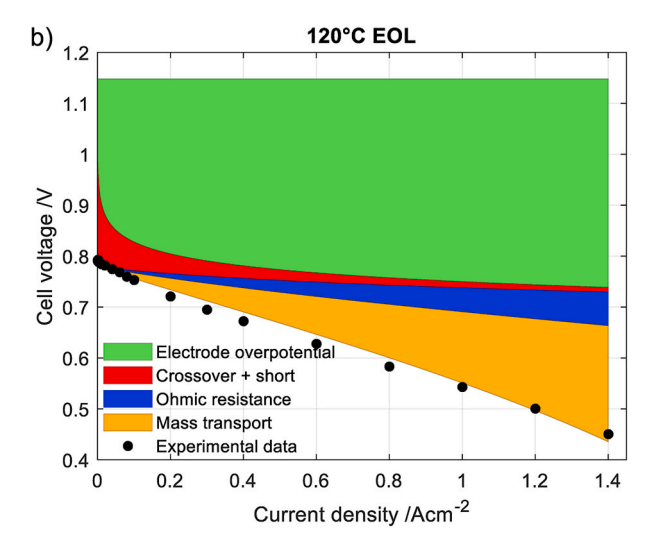


Fig. 7. Polarization curves at a) BOL, and b) EOL 120 °C with the calculated distribution of losses. Measurements were done at SP and 70 % RH, 3 bar ab pressure, with H₂ and air with flow rates of 265 ml min⁻¹ and 662 ml min⁻¹. For the sample at 120 °C the EOL was reached after 72 h.

should be considered that the test had reached the failing criteria, which was triggered by the too low voltage measured, therefore quantitative information cannot be extrapolated from the G-EIS spectra. For all the conditions, G-EIS measurements are in good agreement with the corresponding polarization curves.

3.3. Component-level analysis

The evolution of degradation characterized every 12 h, are displayed in Fig. 5, including the cell voltage at full load (Fig. 5a), hydrogen crossover from linear sweep voltammetry (Fig. 5b), membrane resistance from the HFR of the H₂/air GEIS (Fig. 5c) electrode ionic resistance from H₂/N₂ EIS (Fig. 5d) and catalyst surface ESCA from COstripping (Fig. 5e). Although there is a variation among the repetitions in the absolute values (Fig. S6), despite very similar performance at BOL (Fig. 1a), the trends are the same. The main difference with temperature is observed for hydrogen crossover (Fig. 5b) and cathode ionomer resistance (Fig. 5d). Regarding the samples tested at 80 °C, the analysis shows that the most significant change between BOL and EOL in the first run was the 10 % loss of initial ECSA over time (Fig. 5e). A shift to lower CO-peak potentials and a broadening of the CO peak, which is often related to larger particle sizes [33] was also observed, and confirmed with TEM, discussed below. A faster voltage drop (measured during the polarization curve within the H₂/air characterization step) over time was recorded for the repetition (darker blue color in Fig. S6). This increase in ageing can be attributed mainly to the increase of the resistance of the ionomer over time as shown in Fig. 5c and d, obtained from the G-EIS and P-EIS data.

For the samples aged at 100 °C several causes for ageing can be found. Firstly, an increase in the resistance of the ionomer over time was observed, Fig. 5d. Secondly, an increase in hydrogen crossover, Fig. 5b, was observed, with one sample forming pinholes large enough to cause a large increase in crossover after 96 h. Compared to 80 °C, a faster increase in the HFR, Fig. 5c is also measured for the two samples tested at 100 °C. These results suggest that at 100 °C the polymer is not stable and degrades more rapidly.

For the samples aged at 120 °C, a large increase in hydrogen cross-over was observed (Fig. 5b), due to pinholes formation and these caused the termination of the ageing measurements. The abrupt crossover increase happened around 60 h for both samples. A minor increase in the loss of ECSA at 120 °C compared to 80 °C and 100 °C was also noted, as shown in Fig. 5e. Surprisingly, no increase in the resistance of the ionomer, Fig. 5d, was observed. This might be due to the measurements being terminated prior to degradation being noticeable, or to the

pinholes compromising the validity of the other measurements.

For the samples aged at 100 °C and half load similar ageing as for full load is observed. From the hydrogen crossover, Fig. 5b, the half load samples developed pinholes at around 132 h which is later than the one sample at 100 % load at 100 h. This might suggest that a higher load can accelerate the membrane ageing, but the main cause of pinhole formation is due to elevated temperatures, which is in agreement with the tests at 120 °C and full load. The HFR, Fig. 5c, show no large variations between the two loads, with both increasing at approximately the same rate. For the resistance of the ionomer, Fig. 5d, the half load sample shows no increase while the full load sample shows a large increase over time. If the increased load is causing an increase in the ionomer resistance, this could be due to the lower cathode potential at the higher load, or due to higher local temperatures at higher current densities which are observed to compromise the ionic conductivity also in the membrane. At half load, the cold soak improved the performance as shown in Fig. 2b. On the contrary, at full load such recovery could not be observed, likely due to an irreversible loss in the ionic conductivity of the cathode catalyst layer. However, a higher ionomer resistance should cause a larger loss in performance which was not observed in the polarization curves at SP, as seen in Fig. 3. The measured ECSA and COpeak position for the half load decreased over time, similar to the full load, Fig. 5e, suggesting that the two operating potentials are similar enough not to cause higher rates of Pt oxidation, dissolution or agglomeration, as this would shift and reduce the peak [11,20,34].

The sudden increase in crossover is not notable in the cell voltage that declines more continuously. The about 50 % increase in cell resistance (HFR) and ionomer resistance (R $_{\rm H+}$) during the study, observed at least for 100 °C, indicate that the voltage loss is mainly an effect of polymer electrolyte changes with rising temperature.

3.4. Microscopy evaluation

Microscopy evaluation of the fresh and tested cathodes using STEM-EDS mapping revealed small changes (see Table 2). Visually, as shown in Fig. 6, the cathodes show comparable microstructure and component distribution at the low and high magnification. In these measurements the full cross-sections of the membranes were not mapped and should not be considered here. Some electrode thinning is evident in all tested MEAs. The quantification of the EDS maps showed some differences (Table 2). All electrodes show a thinning of about 10 % on average, as well as a total porosity loss of 10 %, compared to the fresh samples, and no substantial change in Pt loading. The histograms of the size distribution in Fig. 6f are very similar for all samples. The distribution of the F

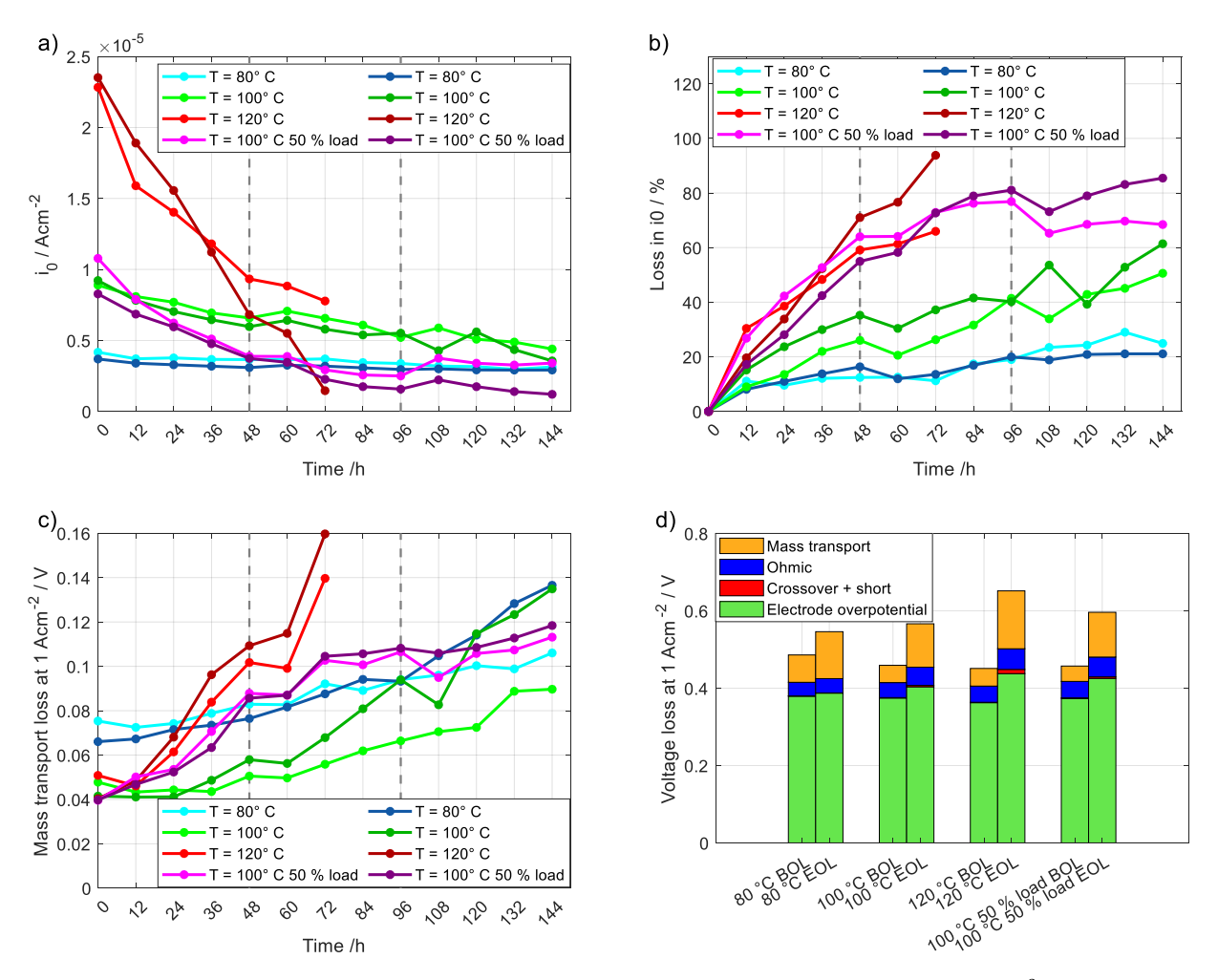


Fig. 8. Changes in fitted values for a) i_0 , b) i_0 percentage, and c) mass transport over time. d) Distribution of total losses at 1 A cm⁻² at BOL and EOL. Measurements were done at 70 % RH, 3 bar ab pressure, with H₂ and air with flow rates of 265 ml min⁻¹ and 662 ml min⁻¹. For the sample at 120 °C the EOL was reached after 72 h.

containing ionomer is less homogeneous after fuel cell operation, however, it is hard to tell whether this is more evident at higher temperatures. Pt particle size increased on average $10\,\%$, from 4.74 to $5.22\,\mathrm{nm}$. Furthermore, after ageing large agglomeration of Pt could be observed in some spots. The small difference between samples confirms that the degradation of the catalyst is not a major cause of the failure at higher temperatures.

The largest change was noticed in terms of calculated ionomer loading and I/C ratio, and an average increase of 44 % and 60 %, respectively, was calculated compared to the fresh cathode. These values are larger at 120 $^{\circ}\text{C}$ compared to 80 $^{\circ}\text{C}$ and 100 $^{\circ}\text{C}$. The ionomer loading and I/C ratio are calculated from the measured fluorine EDS net counts, assuming Nafion composition. The increase in the loading and I/C ratio are a consequence of the higher measured fluorine EDS signal. This increase is most likely caused by the membrane degradation and side chain leaching to the cathode.

3.5. 0-D model of polarization losses

To further elaborate and deduce the contribution and sources of the losses the 0-D model shown in equation (1) was used in which i_0 , i_L and B_c were fitted for each curve measured at the SP. The fitted results and the distribution for the 120 °C sample are shown in Fig. 7, the remaining temperatures are shown in the supporting information, Fig. S9. As can be seen, the model fits the data well, suggesting that the main losses are accounted for in the model. As expected, the main loss for all the

samples, already from the BOL, is from the cathodic overpotential (green area). A relatively small contribution is given by the ohmic losses, which can be linked to the thin membranes ($10~\mu m$) and adequate humidification. The mass transport losses are significant, even at lower current densities. However, it must be noted that the empirical term B_c had to be utilized to allow a good fit, and it does not represent an exact physical phenomenon, but rather the sum of all inhomogeneities and current concentrations in the electrode. However, it suggests that improving the current distribution in the electrodes can significantly improve performance. After ageing, it can be seen that all samples have increases in all losses. However, the largest increase is due to the increase in mass transport resistance. Which is most likely caused by larger current distributions in the electrode and uneven distribution of ionomer as found by TEM. Given the formation of pinholes, the losses due to crossover are noticeably increased at EOL (red area).

The evolution of the fitted parameters i_0 and the combined mass transport losses with time are summarized in Fig. 8. The choice of using the total mass transport instead of i_L and B_C is due to the two constants being indistinguishable from each other in such a simple model and would require other measurements to deconvolute the separate contributions.

The calculated i_0 at the start of the measurements shows an increase of 2.3 and 5.8 times at 100 °C and 120 °C, respectively compared to 80 °C, which is expected as reaction kinetics are improved with temperature [24,35,36], as shown in Fig. 8a. The calculated activation energy using an Arrhenius expression is 50 kJ mol^{-1} , is similar to previous

reported values [35]. Over time the calculated i_0 decreases for all samples, losing approximately 20, 50, 70 and 70 % for the 80, 100, 120 °C and 100 °C at half load respectively (Fig. 8b). The losses can partially be attributed to the loss in ECSA. As the CO-peak position shifted to slightly lower potentials and reduced in size it is attributed to Pt agglomeration, which was confirmed through STEM-EDS [33]. However, as the ECSA loss was less than 20 % for all samples this cannot fully explain the loss in the calculated i_0 , which is significantly larger than 20 %. Thus, the losses are due to more nonuniform current distribution resulting in an apparent drop in exchange current density.

The calculated mass transport loss at 1 A cm⁻², shown in Fig. 8c, shows that the 80 °C sample had a slightly higher mass transport resistance at the start of the measurement compared to the tests at higher temperatures. This is due to the lower saturation pressure of water most likely resulting in local flooding in the electrode. Over the measurements the mass transport loss increases for all tested samples causing large increases in the total losses of the fuel cell. The changes in the losses from BOL to EOL at 1 A cm⁻² for the tested samples are summarized in Fig. 8d. For all samples, the mass transport loss has the largest increase in voltage loss observed in the polarization curves, which is in agreement with the previously discussed Fig. 5d and e and with the I/C ratio measured at EOL. For the changes in cathode overpotential a trend can be observed, with a larger change occurring at higher temperatures, suggesting that while the initial catalyst activity is improved at elevated temperature, the catalyst layer degradation is much faster, resulting in a net loss of activity.

3.6. Final considerations

Degradation cannot be totally avoided during prolonged fuel cell operation. The combination of high load, temperature and pressure, which have been experimentally shown to shorten the PEMFC lifetime, are the most probable for higher temperature operation, at least during high-power demand sections. Therefore, a more careful analysis is required. Although in these tests the effect of load cycling was purposely not included, the periodic characterization of the cell required changes in the operating conditions which have contributed, and probably even partially accelerated the cell degradation. These changes included gas switches, flow changes, RH cycling induced by electrochemical produced water during polarization curves, cold soaks, temperature changes from the RC to the SP. Furthermore, as the formation of pinholes or tears cannot be exactly predicted statistical analysis of degradation becomes difficult.

As concluded in the previous sections, an increased temperature negatively influences the lifetime. The mean rate of degradation, of both repetitions, at full load was 0.63/1.0/3.0/1.0 m Vh⁻¹ at setpoint and $0.7/1.0/0.6/0.7 \text{ m Vh}^{-1}$ at reference conditions for the 80/100/120/100 half load samples respectively. While the degradation rate in this study is high the operating conditions and load were chosen due to their harsh nature. While the reaction kinetics is improved at higher temperatures, leading to a decrease of the cathodic overpotential of about 17 mV at 1 A cm⁻², the equilibrium potential is simultaneously decreased by 34 mV, which negates the effect. To compensate for the higher water saturation pressure, a high total pressure was maintained to ensure adequate dry gas partial pressure, as observed in our previous work [24]. That increased the gas crossover rate, which at higher temperatures are also facilitated by an increased membrane permeability [37]. This enhanced the formation of radicals which are known to attack the membrane chemistry and that are the main responsible for chemical degradations [8]. It is likely that an increase in temperature further enhanced the kinetics of these reactions, causing even larger losses. Therefore, the primary reason for the test failures can be attributed to the degradation of the polymer electrolyte both in membrane and in catalyst layers.

In parallel, a degradation of the functionality of the polymer used as a membrane and as ionomer in the catalyst layer was observed, which

led to reduced ionic conductivity (and therefore increase membrane and cathodic resistivity), Fig. 5c and d. This process was also seen to be accelerated at a higher temperature. Interestingly, the test performed at half load showed that the protonic conductivity of the membrane and ionomer was not affected as much, which resulted in a partial reversible degradation (Fig. 3d vs Fig. 4b) at the RC. Ionomer degradation, or changes in ionomer wetting properties, could lead to more uneven current distribution in the electrode which in turn explains the apparent change in the exchange current density for all samples.

The half load caused larger losses compared to full load. This is attributed to the prolonged hold at higher potentials which might have affected the catalyst and the carbon support to a larger extent. A larger thinning of the catalyst layer of this sample was observed by TEM. Higher temperatures are also reported to accelerate the carbon corrosion and the Pt agglomeration [13], which can be observed in the CO-peak shift to lower potentials. This couples well with the results of our model where the diminished efficient exchange current density, is more severe, as the temperature is raised.

However, above a certain current density, pure activation losses cannot justify the drop in performance seen in the polarization curves, and the losses are due to mass transport related phenomena. In the 0-D model this term includes all the remaining losses, such as current distribution in the electrode and mass transport of reactants and products. The reduced ionic conductivity in the catalyst layer observed through H₂/N₂ P-EIS can partly explain this term. A possible explanation is that the electrode structure has changed its porosity by roughly 10 % for all samples, making it more difficult for the gas diffusion in the catalyst layer. This can also be qualitatively observed in the electrochemical characterization by the appearance and growth of a second semicircle in the low frequency region for the G-EIS. Similarly, porosity and wettability of the GDL might have changed. Additionally, the 0-D model is a simple schematization of the fuel cell, and its assumptions might not be true for the entire experiment, i.e. that the current distribution over the geometric area is uniform. Inhomogeneities would result in local hotspots which locally increase the chance for pinhole formation, carbon corrosion and thermal stresses. These inhomogeneities are likely increasing at higher temperatures, which can explain why the mass transport coefficient is overestimated by the model at higher temperatures.

It is obvious from these results that the state-of-the-art MEAs are not designed for these elevated temperatures and new materials must be developed for this temperature range. Further, more analyses of the structure changes in the catalyst layer have to be made in order to better ascertain the source of the losses in current polymer electrolytes. This paper gives a good reference point and methodology for future studies of novel polymer electrolytes fuel cells designed for elevated temperatures.

4. Conclusions

In this study steady state measurements at high power and high pressure were performed at 80, 100, and 120 $^{\circ}\text{C}$. The results showed that an increased temperature caused an increase in the performance loss of the cell. The main causes of this performance loss were associated with change in the membrane and ionomer. The increased temperature caused an increased hydrogen crossover and likelihood towards pinhole formation in the membrane together with deteriorated ionic conductivity. While increasing the temperature from 80 $^{\circ}\text{C}$ to 100 $^{\circ}\text{C}$ caused an increase in the degradation rate of the cathode ionomer, decreasing the load from full to partial at 100 $^{\circ}\text{C}$ caused the degradation to be in line with 80 $^{\circ}\text{C}$, likely due to a reduced irreversible degradation of the ionic conductivity. On the contrary, the sample aged at half-load showed an enhanced Pt degradation.

The model suggests that the performance decay is to be attributed to increased gas crossover, loss of apparent exchange current density and, more importantly, mass transport limitations, all exacerbated at higher temperatures.

Overall, it can be concluded that, given the current state-of-the-art of the materials, an elevated temperature is negative for the lifetime of a fuel cell. Polymers with better chemical stability, in particular reduced fuel permeability, resistance to radical attacks and prolonged ionic conductivity need to be developed to operate at higher temperatures for prolonged time. The TEM and SEM-ED analysis showed small and similar changes in the electrode thickness and particle sizes for all temperatures meaning that the catalyst is relatively unaffected by the increase in temperature, if the applied current is constant. A remaining challenge is then to address the catalyst layer degradation, including Pt agglomeration, carbon corrosion, and porosity loss at elevated temperatures for a non-constant current load.

Although extended operation at higher temperature is not currently possible, operating at elevated temperatures for shorter durations is feasible.

CRediT authorship contribution statement

B. Eriksson: Writing – original draft, Visualization, Methodology, Investigation, Funding acquisition, Formal analysis, Conceptualization.

M. Butori: Writing – original draft, Visualization, Investigation, Formal analysis, Conceptualization. M. Batool: Investigation. L. Strandberg: Investigation. O. Sanumi: Investigation. S. Pedram: Investigation. B. Wickman: Supervision, Funding acquisition. J. Jankovic: Writing – original draft, Supervision, Investigation, Formal analysis. C. Lagergren: Writing – review & editing, Supervision, Funding acquisition. R. Wreland Lindström: Writing – review & editing, Supervision, Funding acquisition. G. Lindbergh: Writing – review & editing, Supervision, Funding acquisition.

Declaration of competing interest

The authors declare the following financial interests/personal relationships which may be considered as potential competing interests: Björn Eriksson reports financial support was provided by Swedish Energy Agency. Martina Butori reports financial support was provided by Swedish Foundation for Strategic Research. Linnea Strandberg reports financial support was provided by Swedish Foundation for Strategic Research. Björn Wickman reports financial support was provided by Swedish Foundation for Strategic Research. Carina Lagergren reports financial support was provided by Swedish Foundation for Strategic Research. Rakel Wreland Lindstrom reports financial support was provided by Swedish Foundation for Strategic Research, Goran Lindbergh reports financial support was provided by Swedish Foundation for Strategic Research. Carina Lagergren reports financial support was provided by STandUP for Energy. Rakel Wreland Lindström reports financial support was provided by STandUP for Energy. Göran Lindbergh reports financial support was provided by STandUP for Energy. Carina Lagergren reports financial support was provided by Swedish Energy Agency. If there are other authors, they declare that they have no known competing financial interests or personal relationships that could have appeared to influence the work reported in this paper.

Acknowledgments

This work was supported by the Swedish Foundation for Strategic Research (SSF): PUSH - Production, Use, and Storage of Hydrogen (Project number ARC19-0026), the Swedish Energy Agency via Swedish Electromobility Centre (SEC) and Strategic Vehicle Research and Innovation (FFI) and the Swedish governmental initiative StandUp for Energy.

Appendix A. Supplementary data

Supplementary data to this article can be found online at https://doi.org/10.1016/j.jpowsour.2025.238258.

Data availability

Data will be made available on request.

References

- [1] D.A. Cullen, K.C. Neyerlin, R.K. Ahluwalia, R. Mukundan, K.L. More, R.L. Borup, A. Z. Weber, D.J. Myers, A. Kusoglu, New roads and challenges for fuel cells in heavy-duty transportation, Nat. Energy 6 (2021) 462–474.
- [2] M.F. Mathias, R. Makharia, H.A. Gasteiger, J.J. Conley, T.J. Fuller, C.J. Gittleman, S.S. Kocha, D.P. Miller, C.K. Mittelsteadt, T. Xie, S.G. Yan, P.T. Yu, Two fuel cell cars in every garage? Electrochem. Soc. Interface (2005).
- [3] Y. Wang, D.F. Ruiz Diaz, K.S. Chen, Z. Wang, X.C. Adroher, Materials, technological status, and fundamentals of PEM fuel cells – a review, Mater. Today 32 (2020) 178–203.
- [4] P.C. Okonkwo, I. Ben Belgacem, W. Emori, P.C. Uzoma, Nafion degradation mechanisms in proton exchange membrane fuel cell (PEMFC) system: a review, Int. J. Hydrogen Energy 46 (2021) 27956–27973.
- [5] J. Wu, X.Z. Yuan, J.J. Martin, H. Wang, J. Zhang, J. Shen, S. Wu, W. Merida, A review of PEM fuel cell durability: degradation mechanisms and mitigation strategies, J. Power Sources 184 (2008) 104–119.
- [6] Y. Prykhodko, K. Fatyeyeva, L. Hespel, S. Marais, Progress in hybrid composite Nafion®-based membranes for proton exchange fuel cell application, Chem. Eng. J. 409 (2021).
- [7] C. Chen, T.F. Fuller, The effect of humidity on the degradation of Nafion® membrane, Polym. Degrad. Stabil. 94 (2009) 1436–1447.
- [8] M. Zatoń, J. Rozière, D.J. Jones, Current understanding of chemical degradation mechanisms of perfluorosulfonic acid membranes and their mitigation strategies: a review, Sustain. Energy Fuels 1 (2017) 409–438.
- [9] H.L. Nguyen, J. Han, X.L. Nguyen, S. Yu, Y.-M. Goo, D.D. Le, Review of the durability of polymer electrolyte membrane fuel cell in long-term operation: main influencing parameters and testing protocols, Energies 14 (2021).
- [10] M. Obermaier, K. Jozwiak, M. Rauber, A. Bauer, C. Scheu, Comparative study of pinhole detection methods for automotive fuel cell degradation analysis, J. Power Sources 488 (2021).
- [11] E. Wallnöfer-Ogris, F. Poimer, R. Köll, M.-G. Macherhammer, A. Trattner, Main degradation mechanisms of polymer electrolyte membrane fuel cell stacks – mechanisms, influencing factors, consequences, and mitigation strategies, Int. J. Hydrogen Energy 50 (2024) 1159–1182.
- [12] K.A. Page, K.M. Cable, R.B. Moore, Molecular origins of the thermal transitions and dynamic mechanical relaxations in perfluorosulfonate ionomers, Macromolecules 38 (2005) 6472–6484.
- [13] K. Kakinuma, H. Taniguchi, T. Asakawa, T. Miyao, M. Uchida, Y. Aoki, T. Akiyama, A. Masuda, N. Sato, A. Iiyama, The possibility of intermediate-temperature (120 °C)-operated polymer electrolyte fuel cells using perfluorosulfonic acid polymer membranes, J. Electrochem. Soc. 169 (2022).
- [14] P. Parthasarathy, A.V. Virkar, Electrochemical Ostwald ripening of Pt and Ag catalysts supported on carbon, J. Power Sources 234 (2013) 82–90.
- [15] S. Cherevko, N. Kulyk, K.J.J. Mayrhofer, Durability of platinum-based fuel cell electrocatalysts: dissolution of bulk and nanoscale platinum, Nano Energy 29 (2016) 275–298.
- [16] P.J. Ferreira, G.J. la O, Y. Shao-Horn, D. Morgan, R. Makharia, S. Kocha, H. A. Gasteiger, Instability of Pt / C electrocatalysts in proton exchange membrane fuel cells: a mechanistic investigation, J. Electrochem. Soc. 152 (2005) A2256–A2271.
- [17] T. Akita, A. Taniguchi, J. Maekawa, Z. Siroma, K. Tanaka, M. Kohyama, K. Yasuda, Analytical TEM study of Pt particle deposition in the proton-exchange membrane of a membrane-electrode-assembly, J. Power Sources 159 (2006) 461–467.
- [18] H.-S. Oh, J.-G. Oh, S. Haam, K. Arunabha, B. Roh, I. Hwang, H. Kim, On-line mass spectrometry study of carbon corrosion in polymer electrolyte membrane fuel cells, Electrochem. Commun. 10 (2008) 1048–1051.
- [19] L.M. Roen, C.H. Paik, J.T.D. J, Electrocatalytic corrosion of carbon support in PEMFC cathodes, Electrochem. Solid State Lett. 7 (2004) A19–A22.
- [20] R.L. Borup, A. Kusoglu, K.C. Neyerlin, R. Mukundan, R.K. Ahluwalia, D.A. Cullen, K.L. More, A.Z. Weber, D.J. Myers, Recent developments in catalyst-related PEM fuel cell durability, Curr. Opin. Electrochem. 21 (2020) 192–200.
- [21] G. Tsotridis, A. Pilenga, G. De Marco, T. M, EU HARMONISED TEST PROTOCOLS FOR PEMFC MEA TESTING IN SINGLE CELL CONFIGURATION FOR AUTOMOTIVE APPLICATIONS, vol.27632, EUR, 2015.
- [22] E. Colombo, A. Baricci, A. Bisello, L. Guetaz, A. Casalegno, PEMFC performance decay during real-world automotive operation: evincing degradation mechanisms and heterogeneity of ageing, J. Power Sources 553 (2023).
- [23] E. Colombo, A. Baricci, D. Mora, L. Guetaz, A. Casalegno, An innovative accelerated stress test representative of automotive PEMFC degradation mechanisms validated on 1000 hours real-world operation, J. Power Sources 580 (2023).
- [24] M. Butori, B. Eriksson, N. Nikolić, C. Lagergren, G. Lindbergh, R.W. Lindström, The effect of oxygen partial pressure and humidification in proton exchange membrane fuel cells at intermediate temperature (80–120 °C), J. Power Sources 563 (2023).
- [25] S. Touhami, J. Mainka, J. Dillet, S.A.H. Taleb, O. Lottin, Transmission line impedance models considering oxygen transport limitations in polymer electrolyte membrane fuel cells, J. Electrochem. Soc. 166 (2019) F1209–F1217.
- [26] T. Vidaković, M. Christov, K. Sundmacher, The use of CO stripping for in situ fuel cell catalyst characterization, Electrochim. Acta 52 (2007) 5606–5613.

- [27] M. Jouin, R. Gouriveau, D. Hissel, M.-C. Péra, N. Zerhouni, Degradations analysis and aging modeling for health assessment and prognostics of PEMFC, Reliab. Eng. Syst. Saf. 148 (2016) 78–95.
- [28] A. Colliard-Granero, M. Batool, J. Jankovic, J. Jitsev, M.H. Eikerling, K. Malek, M. J. Eslamibidgoli, Deep learning for the automation of particle analysis in catalyst layers for polymer electrolyte fuel cells, Nanoscale 14 (2021) 10–18.
- [29] N. Macauley, R.D. Lousenberg, M. Spinetta, S. Zhong, F. Yang, W. Judge, V. Nikitin, A. Perego, Y. Qi, S. Pedram, J. Jankovic, I.V. Zenyuk, H. Xu, Highly durable fluorinated high oxygen permeability ionomers for proton exchange membrane fuel cells, Adv. Energy Mater. 12 (2022).
- [30] A. Kneer, J. Jankovic, D. Susac, A. Putz, N. Wagner, M. Sabharwal, M. Secanell, Correlation of changes in electrochemical and structural parameters due to voltage cycling induced degradation in PEM fuel cells, J. Electrochem. Soc. 165 (2018) F3241–F3250.
- [31] T.R. Garrick, T.E. Moylan, V. Yarlagadda, A. Kongkanand, Characterizing electrolyte and platinum interface in PEM fuel cells using CO displacement, J. Electrochem. Soc. 164 (2016) F60–F64.
- [32] K. Shinozaki, H. Yamada, Y. Morimoto, Relative humidity dependence of Pt utilization in polymer electrolyte fuel cell electrodes: effects of electrode Thickness, Ionomer-to-Carbon ratio, ionomer equivalent weight, and carbon support, J. Electrochem. Soc. 158 (2011).

- [33] E.G. Ciapina, S.F. Santos, E.R. Gonzalez, Electrochemical CO stripping on nanosized Pt surfaces in acid media: a review on the issue of peak multiplicity, J. Electroanal. Chem. 815 (2018) 47–60.
- [34] V. Shokhen, L. Strandberg, M. Skoglundh, B. Wickman, Impact of accelerated stress tests on the cathodic catalytic layer in a Proton Exchange Membrane (PEM) fuel cell studied by identical location scanning electron microscopy, ACS Appl. Energy Mater. 5 (2022) 11200–11212.
- [35] N. Wakabayashi, M. Takeichi, M. Itagaki, H. Uchida, M. Watanabe, Temperature-dependence of oxygen reduction activity at a platinum electrode in an acidic electrolyte solution investigated with a channel flow double electrode, J. Electroanal. Chem. 574 (2005) 339–346.
- [36] H. Yano, J. Inukai, H. Uchida, M. Watanabe, P.K. Babu, T. Kobayashi, J.H. Chung, E. Oldfield, A. Wieckowski, Particle-size effect of nanoscale platinum catalysts in oxygen reduction reaction: an electrochemical and 195Pt EC-NMR study, Phys. Chem. Chem. Phys. 8 (2006) 4932–4939.
- [37] M. Butori, B. Eriksson, N. Nikolić, C. Lagergren, G. Lindbergh, R. Wreland Lindström, Ionic conductivity and hydrogen crossover for IT-PEMFCs: influence of pressure, temperature, relative humidity and reinforcement, Int. J. Hydrogen Energy 95 (2024) 1158–1170.